Crystallization behaviour of amorphous $Fe_{73.5}Cu_1Nb_3Si_{13.5}B_9$



1992 J. Phys.: Condens. Matter 4 10295

(http://iopscience.iop.org/0953-8984/4/50/017)

J. Phys.: Condens. Matter 4 (1992) 10295–10310. Printed in the UK

# Crystallization behaviour of amorphous $Fe_{73.5}Cu_1Nb_3Si_{13.5}B_9$

Georg Rixeckert, Peter Schaaf‡§ and Ulrich Gonsert

† Universität des Saarlandes, Werkstoffwissenschaften, D-6600 Saarbrücken, Federal Republic of Germany

‡ II. Physikalisches Institut der Universität Göttingen, Bunsenstraße 7–9, D-3400 Göttingen, Federal Republic of Germany

Received 20 August 1992, in final form 13 October 1992

**Abstract.** Iron-based amorphous alloys have attracted technological and scientific interest due to their soft magnetic properties. Recently it was found that amorphous alloys like $Fe_{73.5}Cu_1Nb_3Si_{13.5}B_9$ (FINEMET™) have a transition to the nanocrystalline state after proper annealing, thus exhibiting excellent magnetic properties.

An attempt was made to investigate the crystallization behaviour of this alloy, which is not yet fully known. The investigation was carried out by combining several methods, namely Mössbauer spectroscopy, x-ray diffraction, scanning and transmission electron microscopy as well as microprobe analysis.

The alloy was studied after annealing at various temperatures for various times. The corresponding phase analyses are presented. Even after increasing the time of annealing at 950°C from 1 h to 90 h significant changes in the phases were found.

It became evident that the question of phase composition can be solved only by a combination of different methods .

## 1. Introduction

Soon after the discovery of the excellent soft magnetic properties of the properly annealed iron-based amorphous alloy FINEMET ($Fe_{73.5}Cu_1Nb_3Si_{13.5}B_9$) by Yoshizawa, Oguma and Yamauchi [1] this alloy began to attract great scientific interest. In the aftermath many publications on the origin of the magnetic properties of $Fe_{73.5}Cu_1Nb_3Si_{13.5}B_9$ and related alloys appeared; here only some of the references are given [2–7].

The soft magnetic properties of FINEMET are attributed to the ultrafine grain structure revealed after annealing for one hour at about 550°C. The existence and thermal stability of this microstructure with a mean grain size of the order of 10 nm are due to the presence of Cu and Nb [1, 4].

While this first crystallization stage and the origin of the soft magnetic properties are well known, the crystallization behaviour upon extended thermal treatment is not definitely known, though phase analyses have repeatedly been undertaken [8–13]. Therefore an attempt was made to investigate the crystallization behaviour of $Fe_{73.5}Cu_1Nb_3Si_{13.5}B_9$ by a combination of several methods on the supposition that they would provide complementary information.

§ Formerly of Universität des Saarlandes, Werkstoffwissenschaften, D-6600 Saarbrücken, Federal Republic of Germany.

0953-8984/92/5010295+16$07.50  

Among the methods used for this study was Mössbauer spectroscopy because it has been successfully applied in many investigations of amorphous and nanocrystalline iron-based alloys [14, 15].

## 2. Experimental details

The amorphous $Fe_{73.5}Cu_1Nb_3Si_{13.5}B_9$ samples were prepared by the melt spinning technique and provided by Dr H R Hilzinger, Vakuumschmelze GmbH, Hanau. These amorphous ribbons have a width of 15 mm and a thickness of 20 $\mu$m.

Annealing was carried out in a vacuum furnace at a pressure of 5 mPa. The annealing temperatures and times are given in table 1.

**Table 1.** Annealing temperatures $T_a$ and annealing times $t_a$ of the samples under investigation.

| Id. | $T_a$ | $t_a$ | Microstructure |
|---|---|---|---|
| A | — | — | Fully amorphous, as-quenched |
| B | 550 °C | 1 h | Nanocrystalline, amorphous |
| C | 700 °C | 1 h | Crystalline (amorphous remains?) |
| D | 950 °C | 1 h | Fully crystalline |
| E | 950 °C | 90 h | Fully crystalline |

The samples were investigated using Mössbauer spectroscopy, x-ray diffration (XRD), scanning electron microscopy (SEM), transmission electron microscopy (TEM) and energy dispersive x-ray analysis (EDX).

Mössbauer spectroscopy was carried out at room temperature in transmission geometry using a constant acceleration drive and a $^{57}Co$ in Rh source with an activity of 400–950 MBq. Calibration was made using $\alpha$-Fe foil, and isomer shifts are given relative to $\alpha$-Fe.

The nanocrystalline and crystalline spectra were analysed with a least-squares program [16] by superimposing sets of Lorentzian lines. Due to a restriction of this program, the amorphous phase occurring in the nanocrystalline sample had to be fitted by pseudo-Lorentzian lines [17, 18].

X-ray diffraction was carried out on various diffractometers using Mo K$\alpha$ and Co K$\alpha$ radiation.

## 3. Results and discussion

The Mössbauer spectra of the $Fe_{73.5}Cu_1Nb_3Si_{13.5}B_9$ ribbon in its various annealing states are shown in figure 1. Better resolved spectra will be given separately for a detailed discussion.

These spectra reveal the transformation from the initial amorphous state (figure 1(*a*)) to crystalline states with increasing annealing temperature $T_a$. Even at an annealing temperature of 950 °C one can see significant changes if the annealing time is increased from $t_a = 1$ h to $t_a = 90$ h (figure 1(*e*)).

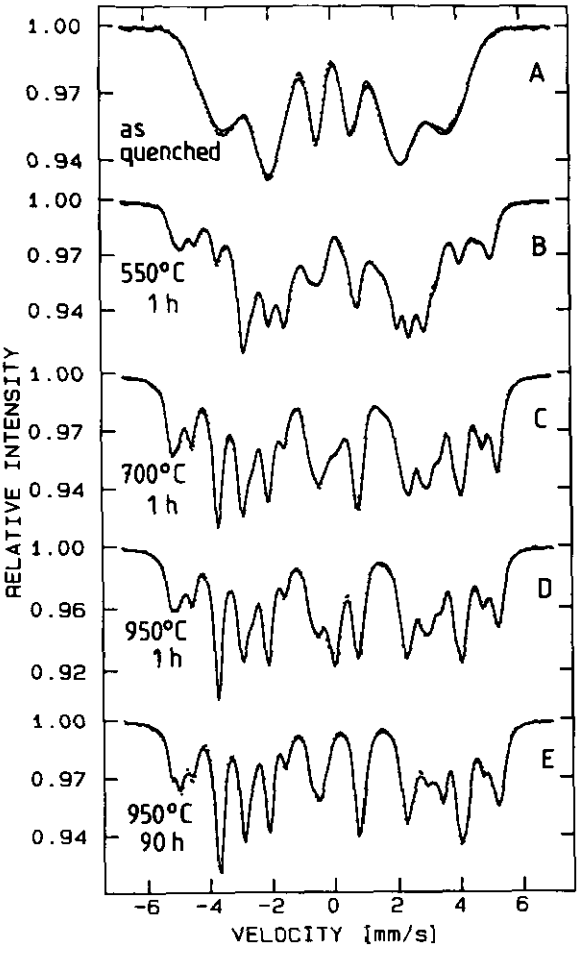


**Figure 1.** Transmission Mössbauer spectra of $Fe_{73.5}Cu_1Nb_3Si_{13.5}B_9$ after various annealing treatments. $T_a$ and $t_a$ are given for each spectrum.

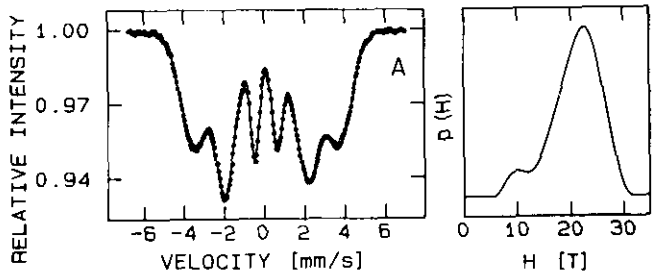


**Figure 2.** Transmission Mössbauer spectrum of the as-quenched amorphous $Fe_{73.5}Cu_1Nb_3Si_{13.5}B_9$ ribbon (sample A). The distribution of the hyperfine field $p(H)$ is given on the right.

### *3.1. Sample A: amorphous $Fe_{73.5}Cu_1Nb_3Si_{13.5}B_9$*

The Mössbauer spectrum of the as-cast amorphous $Fe_{73.5}Cu_1Nb_3Si_{13.5}B_9$ ribbon is shown in figure 2.

This spectrum exhibits the well known characteristics of an amorphous spectrum. It was fitted according to the Hesse–Rübartsch method [19] with the program of LeCaer *et al* [20]. The mean hyperfine field was calculated to be $\bar{H} = 207$ kOe, the isomer shift $\delta = 0.10\,\mathrm{mm\,s^{-1}}$.

### *3.2. Sample B: $Fe_{73.5}Cu_1Nb_3Si_{13.5}B_9$, 550 °C, 1 h*

The amorphous $Fe_{73.5}Cu_1Nb_3Si_{13.5}B_9$ ribbon was annealed at 550°C for 1 h, the annealing treatment which leads to the excellent soft magnetic properties [1]. The corresponding Mössbauer spectrum is given in figure 3. The hyperfine parameters of the subspectra as revealed by the numerical analysis are given in table 2. The same nomenclature for the subspectra is used in both the figure and the table.

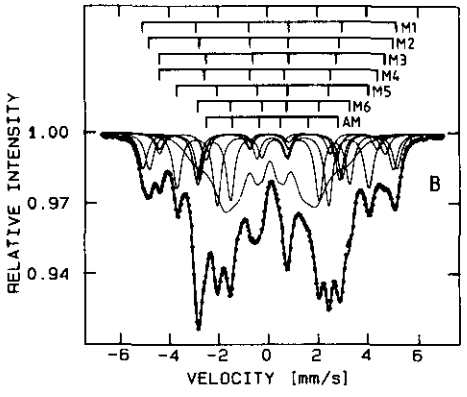


**Figure 3.** Transmission Mössbauer spectrum of sample B: $Fe_{73.5}Cu_1Nb_3Si_{13.5}B_9$ annealed at 550 °C for 1 h.

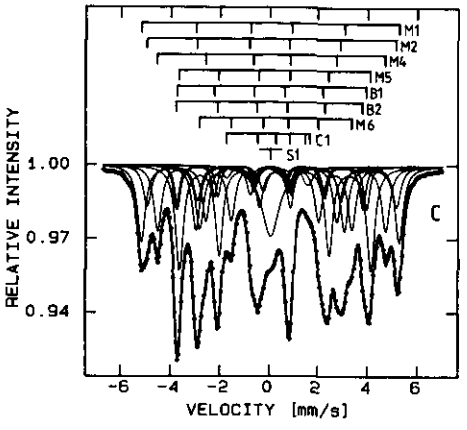


**Figure 4.** Transmission Mössbauer spectrum of sample C: $Fe_{73.5}Cu_1Nb_3Si_{13.5}B_9$ annealed at 700 °C for 1 h.

**Table 2.** Hyperfine parameters as obtained for sample B: $Fe_{73.5}Cu_1Nb_3Si_{13.5}B_9$, 550 °C/1 h.

| Sub-spectrum | $\delta$ (mm $s^{-1}$) | QS (mm $s^{-1}$) | H (kOe) | $\Gamma$ (mm $s^{-1}$) | RA (%) |
|---|---|---|---|---|---|
| M1 | 0.04 | 0.00 | 317 | 0.40 | 10.6 |
| M2 | 0.07 | 0.02 | 305 | 0.40 | 11.5 |
| M3 | 0.13 | 0.00 | 283 | 0.40 | 6.3 |
| M4 | 0.00 | 0.03 | 272 | 0.40 | 5.3 |
| M5 | 0.18 | 0.00 | 241 | 0.40 | 16.5 |
| M6 | 0.24 | −0.02 | 191 | 0.40 | 11.6 |
| AM† | 0.13 | 0.05 | 169 | 2.00 | 38.3 |

† Pseudo-Lorentzian profile with $\alpha = 3.35$.

The analysis of the Mössbauer spectrum of nanocrystalline FINEMET yields two phases: an amorphous phase with a reduced hyperfine field $\bar{H} = 169$ kOe denoted by AM and the iron–silicon phase with $Fe_3Si$ structure (subspectra M1–M6).

The mean hyperfine field of the amorphous phase is reduced in comparison with the initial amorphous state. Annealing of an amorphous alloy normally leads to an enhanced hyperfine field due to an increase in density. Here the amorphous phase is depleted in iron thus exhibiting a decreased hyperfine field.

Up to 10 at.% silicon is soluble in BCC iron, randomly substituting iron atoms. A further increase of the silicon content leads to a phase transition towards the ordered $DO_3$ structure which exists between about 10 at.% and 30 at.% Si [21,22]. Both

phases, disordered and ordered, have been investigated by Mössbauer spectroscopy [23–27]. As the $DO_3$ phase plays an important role in the Mössbauer phase analysis of the $Fe_{73.5}Cu_1Nb_3Si_{13.5}B_9$ ribbons, it must be discussed here in detail.

The lattice parameter of the $D0_3$ crystal structure is roughly twice as large as that of $\alpha$-iron, the unit cell consisting of 16 atoms. Two cubic sublattices are present: one of these, designated as A, consists of 8 iron atoms, whereas the other, D, contains both iron and silicon. In the stoichiometric compound $Fe_3Si$, the sublattice D is completely ordered, thus containing equal numbers of $D_{Fe}$ and $D_{Si}$ sites.

In Mössbauer spectra of Fe–25 at.%Si alloy, two subspectra are present corresponding to Fe atoms at A and $D_{Fe}$ sites, respectively.

If the silicon content $c$ is less than 25 at.%, Fe atoms will occupy some of the $D_{Si}$ sites randomly, thus giving additional iron sites. Their probabilities can be calculated using the binomial distribution

$$A_n = A(n,0) = [0.5/(1-c)]\binom{4}{n}(4c)^n(1-4c)^{4-n} \qquad n = 0\ldots4 \tag{1}$$

$$D_n = D(0,n) = [(0.5-c)/(1-c)]\,(0.25)/(0.5-c)\binom{6}{n}(4c)^n(1-4c)^{6-n} \qquad n = 1\ldots6 \tag{2}$$

$$D_0 = D(0,0) = [(0.5-c)/(1-c)]\,[(0.25-c)/(0.5-c)] + [(0.5-c)/(1-c)]\,[(0.25)/(0.5-c)](1-4c)^6 \tag{3}$$

where $A(n,0)$ represents an iron atom in the A sublattice having n silicon atoms as nearest neighbours, and $D(0,n)$ means an iron atom in the D sublattice having $n$ silicon atoms as next-nearest neighbours.

According to the above formulae, 11 different configurations exist which have different numbers of silicon nearest neighbours and/or silicon next nearest neighbours. These configurations can be partially resolved in the Mössbauer spectrum. The silicon content can be calculated if the subspectra can be assigned to the various sites.

The hyperfine parameters of these different iron sites are known to be almost independent of the silicon content of the alloy [25] and are roughly the same for all thermal treatments. The only exception is the nanocrystalline alloy, where all hyperfine splittings are reduced by 2–3 %.

This effect can be attributed to the small grain size which is below the range of the ferromagnetic exchange coupling. Thus, the reduced magnetic field in the amorphous phase exerts a certain influence on the hyperfine field in the Fe–Si phase.

The silicon content in the nanocrystalline Fe–Si phase as calculated from Mössbauer results is 18.6 at.%. It is also possible to calculate the silicon content from an XRD spectrum using the lattice parameter. An increasing silicon content leads to a reduction of the lattice constant $a$, depending linearly on $c_{Si}$. The study reported in [22] covers the concentration range from 12.75 at.% Si ($a$=5.7036 Å) to 31.04 at.% ($a$=5.6266 Å).

Several phase analyses of the nanocrystalline FINEMET have been published, and the presence of the crystalline iron–silicon phase is widely accepted, as well as the presence of the amorphous phase with a reduced content of iron and silicon. The nanocrystalline iron–silicon compound with a mean grain size of 10–20 nm [6, 13] has the $D0_3$ structure of $Fe_3Si$ [10–12] with a silicon content of 16–22 at.% [13, 28, 29].

Other researchers performing x-ray measurements speak only of a BCC iron–silicon phase, thus ignoring the ordered structure $D0_3$ [4, 8, 9].

Zemč´ik *et al* [29] claim the existence of tetragonal $Fe_3B$ as a third phase from their analysis of the Mössbauer spectrum of nanocrystalline $Fe_{73.5}Cu_1Nb_3Si_{13.5}B_9$. Here, no evidence of phases other than those listed in table 2 could be found.

### *3.3. Sample C: $Fe_{73.5}Cu_1Nb_3Si_{13.5}B_9$, 700 °C, 1 h*

Annealing the amorphous $Fe_{73.5}Cu_1Nb_3Si_{13.5}B_9$ ribbon at the higher temperature of 700 °C and also for 1 h yields the Mössbauer spectrum shown in figure 4. The corresponding hyperfine parameters are given in table 3.

**Table 3.** Hyperfine parameters as obtained for sample C: $Fe_{73.5}Cu_1Nb_3Si_{13.5}B_9$, 700 °C/1 h.

| Subspectrum | $\delta$ (mm $s^{-1}$) | QS (mm $s^{-1}$) | H (kOe) | $\Gamma$ (mm $s^{-1}$) | RA (%) |
|---|---|---|---|---|---|
| M1 | 0.05 | 0.00 | 324 | 0.39 | 16.6 |
| M2 | 0.06 | 0.05 | 314 | 0.39 | 9.0 |
| M4 | 0.10 | 0.00 | 287 | 0.39 | 14.2 |
| M5 | 0.23 | 0.02 | 241 | 0.39 | 22.7 |
| M6 | 0.26 | 0.01 | 192 | 0.39 | 13.8 |
| B1 | 0.06 | 0.06 | 238 | 0.28 | 6.5 |
| B2 | 0.06 | −0.04 | 235 | 0.28 | 6.5 |
| C1 | 0.26 | −0.27 | 107 | 0.39 | 2.8 |
| S1 | 0.03 | | | 0.85 | 7.9 |

FINEMET alloys annealed at temperatures between 620 °C and 800 °C have repeatedly been the subject of phase analyses performed by Mössbauer spectroscopy, x-ray diffraction and other methods.

However, only the existence of the $D0_3$-Fe–Si phase is commonly accepted, whereas in the various publications, different borides are mentioned, namely $M_3B$ [8], $Fe_2B$ [9], $Fe_2B$ and $Fe_3B$ [10], $Fe_3(Si,B)$ [11], $Fe_{23}B_6$ and $Fe_2B$ [12], and $Fe_{23}B_6$ [13].

A broad single line, which all authors include in their fits, is thought to be the remainder of the amorphous phase depleted in iron. The chemical composition of this phase, though named Fe–Nb–B [13], was never properly investigated. This phase is marked as S1 in table 3.

In the analysis of the Mössbauer spectrum of the sample annealed at 700 °C, the Fe–Si and $Fe_2B$ phases are present, the hyperfine parameters of the latter phase being in excellent agreement with literature values provided by Alp *et al* [30] and Limbach *et al* [31].

The relative areas of the $Fe_3Si$ phase are in good agreement with a silicon content of 18.4 at.%.

The subspectrum labelled C1 is attributed to $(Fe,Si)_3B$ with the cementite structure $D0_{11}$. This orthorhombic cementite structure, of which the compound $Fe_3C$ is the prototype, has sixteen atoms in the unit cell, two thirds of the 12 metal atoms having 11 metal and 3 metalloid atoms in their neighbourhood, and one third having 12 metal and 2 metalloid atoms as neighbours [32].

Mössbauer parameters are known for $(Fe,M)_3C$, where M indicates the substitution of some Fe by other metals as for example Cr and Mn [33,34], and for orthorhombic $Fe_3B$ [35].

The hyperfine splittings of the two iron sites are known from the investigations above to be 205 kOe and 207 kOe, respectively, for $Fe_3C$ and 235 kOe and 264 kOe, respectively, for o-$Fe_3B$.

With a value of 106 kOe, the hyperfine field attributed to the phase $(Fe,Si)_3B$ is remarkably reduced compared to the above mentionened values for $Fe_3B$. This can be understood if one assumes that in the phase present, a certain amount of iron sites is occupied by substitutional silicon atoms.

In $(Fe,M)_3C$, the transition metal atoms M substitute iron rather than carbon, thus causing a decrease of both the magnetic ordering temperature and the hyperfine splitting at room temperature. For this compound, it was found [34] that the Curie temperature decreases with increasing Mn content from 210 °C initially and reaches room temperature at about 15 at.% Mn. Due to the influence of the Si content on the magnetic ordering temperature, it can be assumed that the corresponding phase must be written as $(Fe,Si)_3B$ rather than $Fe_3(Si,B)$. In the study by Aronsson and Lundgren [36], this question was left open. Further support for the assumption of a phase with cementite structure is provided by the x-ray diffraction study which was performed using Mo K$\alpha$ radiation. The XRD spectrum is shown in figure 5, and the phase analysis is given in table 4.

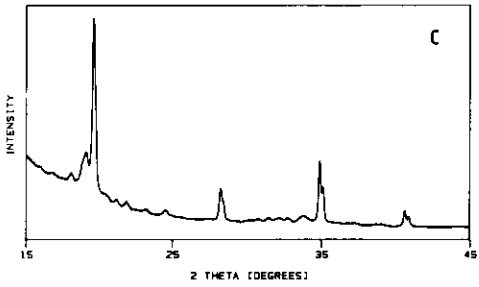


**Figure 5.** XRD spectrum (Mo K$\alpha$) of sample C: $Fe_{73.5}Cu_1Nb_3Si_{13.5}B_9$ annealed at 700 °C for 1 h.

**Table 4.** XRD phase analysis for sample C: $Fe_{73.5}Cu_1Nb_3Si_{13.5}B_9$, 700 °C/1 h.

| Phase | Crystal system | Lattice parameters |
|---|---|---|
| $Fe_{3+x}Si_{1-x}$ | Cubic (FCC) | $a = 5.688$ Å (17 at.% Si) |
| $Fe_2B$ | Tetragonal | $a = 5.140$ Å $c = 4.20$ Å |
| $(Fe,Si)_3B$ | Orthorhombic | $a = 5.380$ Å $b = 6.370$ Å $c = 4.490$ Å |
| Cu | Cubic (FCC) | $a = 3.600$ Å |
| Amorphous | Not indexed | $d = 1.334, 1.309, 1.256, 1.233$ Å |

The presence of elementary copper agrees with the model that Cu precipitates enhance the nucleation of the $D0_3$ Fe–Si grains at an earlier stage of crystallization.

The silicon content of the Fe–Si phase can be calculated from the lattice constant. Here, it was found to be 17 at.%. Four peaks in that diffraction pattern could not be indexed and they are most probably connected with the remainder of the amorphous phase S1. The analysis of the sample heat treated at 950 °C, which will be presented in the next section, will elucidate the nature of the phase which is formed upon its crystallization.

### *3.4. Sample D: Annealing at 950 °C, 1 h*

Figure 6 shows the spectrum of $Fe_{73.5}Cu_1Nb_3Si_{13.5}B_9$ after annealing at $T_a = 950\,°C$ for $t_a = 1$ h. The corresponding hyperfine parameters of the involved subspectra are given in table 5.

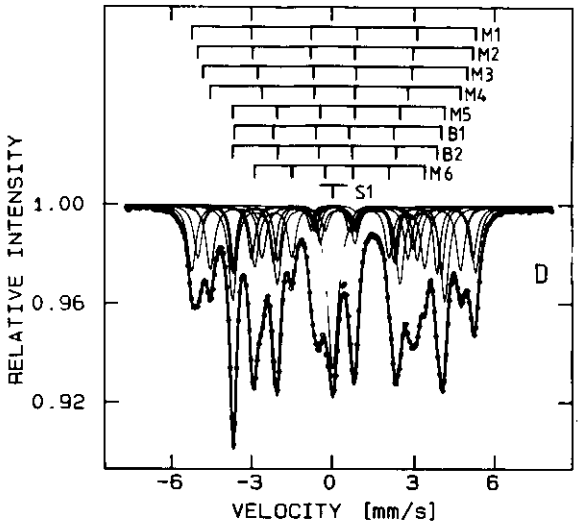


**Figure 6.** Transmission Mössbauer spectrum of sample D: $Fe_{73.5}Cu_1Nb_3Si_{13.5}B_9$ annealed at 950 °C for 1 h.

**Table 5.** Hyperfine parameters as obtained for sample D: $Fe_{73.5}Cu_1Nb_3Si_{13.5}B_9$, 950 °C/1 h.

| Subspectrum | $\delta$ (mm s$^{-1}$) | QS (mm s$^{-1}$) | H (kOe) | $\Gamma$ (mm s$^{-1}$) | RA (%) |
|---|---|---|---|---|---|
| M1 | 0.04 | −0.02 | 327 | 0.35 | 13.0 |
| M2 | 0.05 | 0.04 | 317 | 0.35 | 10.3 |
| M3 | 0.08 | 0.00 | 304 | 0.35 | 3.2 |
| M4 | 0.08 | 0.00 | 288 | 0.35 | 12.6 |
| M5 | 0.20 | 0.01 | 244 | 0.35 | 18.4 |
| M6 | 0.25 | 0.01 | 194 | 0.35 | 12.0 |
| B1 | 0.09 | 0.08 | 239 | 0.27 | 10.2 |
| B2 | 0.09 | −0.03 | 236 | 0.27 | 10.2 |
| S1 | 0.03 | | | 0.49 | 10.2 |

Again, the Mössbauer spectrum consists of the Fe–Si and $Fe_2B$ subspectra which are already known, plus a single line S1 of greatly reduced linewidth compared to sample C, which represents the crystallization product of the remaining amorphous phase. $(Fe,Si)_3B$ is no longer detectable in this state of crystallization. The silicon content of the $D0_3$ phase was calculated to be 18.3 at.% .

In order to obtain more detailed information on the chemical composition of the unknown phase, an electron microscopy investigation was carried out using a Jeol TEM equipped with a scanning facility and a Tracor Northern EDX spectrometer. The specimen thinning was done using ion-beam etching.

Figure 7 shows photographs taken at different magnifications in the normal transmission mode of the instrument.

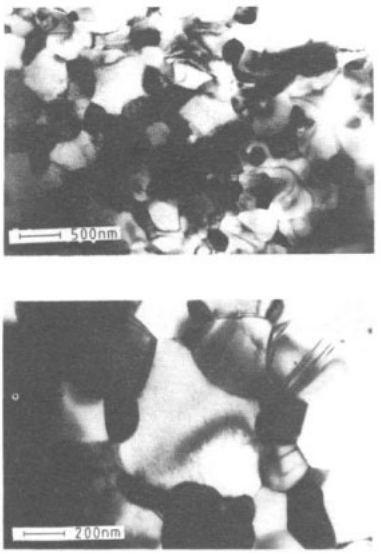


**Figure 7.** TEM images of sample D: $Fe_{73.5}Cu_1Nb_3Si_{13.5}B_9$ annealed at 950 °C for 1 h.

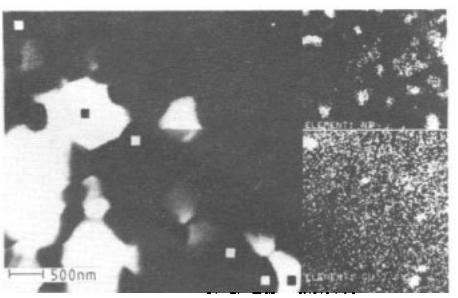


**Figure 8.** Scanning images of sample D: $Fe_{73.5}Cu_1Nb_3Si_{13.5}B_9$ annealed at 950 °C for 1 h. Distribution images: upper right Nb, lower right Cu. Backscattered electron image: The grains marked by □ are (from upper left to lower right) Cu, Fe–Si, Fe–Nb–Si, Cu, Fe–Nb–Si, Fe–Si.

Distribution images were taken, and microanalysis was performed using the analytical capabilities of the TEM. Figure 8 shows a picture taken in backscattered electron mode together with Nb and Cu distribution images (the Nb image showing only the lower part of the imaged area). The small dots in the Cu image represent electronic noise. The phases which were found from these investigations are presented in table 6.

**Table 6.** Microanalysis (EDX) of sample D: $Fe_{73.5}Cu_1Nb_3Si_{13.5}B_9$, 950 °C/1 h.

| | |
|---|---|
| Cu | Several grains identified by comparison of Cu distribution and backscattered electron images |
| Fe–Si | Fe–22±4 at.% Si from EDX analysis |
| Fe–B | Some grains of virtually pure Fe were interpreted as boride grains |
| Fe–Nb–Si | 17 grains analysed by EDX contained Fe, Nb and Si in variable proportions. The mean composition was 66.5±7 at.% Fe, 15.5±5.5 at.% Nb and 18±3 at.% Si |

The Fe–Nb–Si grains were found preferentially surrounding large (up to 1 $\mu$m) Fe–Si grains and were in close contact with these grains. Some mismatch fringes between the two phases could be seen in dark-field images of the respective areas. In order to determine the crystal structure of the Fe–Nb–Si phase, an XRD spectrum was recorded using Co K$\alpha$ radiation. The spectrum is shown in figure 9, and the results are given in table 7.

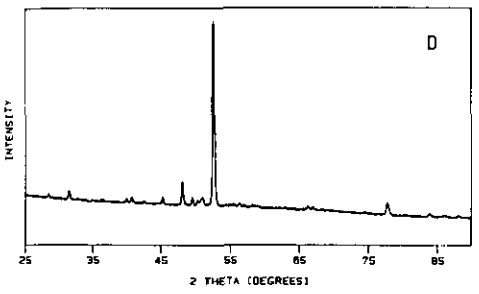


**Figure 9.** XRD spectrum (Cu K$\alpha$) of sample D: $Fe_{73.5}Cu_1Nb_3Si_{13.5}B_9$ annealed at 950 °C for 1 h.

**Table 7.** XRD phase analysis for sample D: $Fe_{73.5}Cu_1Nb_3Si_{13.5}B_9$, 950 °C/1 h

| Phase | Crystal system | Lattice parameters |
|---|---|---|
| $Fe_{3+x}Si_{1-x}$ | Cubic (FCC) | $a = 5.688$ Å (17 at.% Si) |
| $Fe_2B$ | Tetragonal | $a = 5.110$ Å $c = 4.240$ Å |
| $(Fe, Si)_3B$ | Orthorhombic | $a = 5.290$ Å $b = 6.690$ Å $c = 4.480$ Å |
| Cu | Cubic (FCC) | $a = 3.620$ Å |
| Fe–Nb–Si | Cubic (FCC) | $a = 11.34$ Å |

Note that, in contrast to Mössbauer spectroscopy, traces of a phase with cementite structure can be seen in the XRD spectrum. This may be due to a small amount of the $(Fe,Si)_3B$ phase being limited to the surface of the ribbon.

The silicon content of the $D0_3$ phase was calculated from the lattice constant to be 17%.

The niobium-containing phase is found to be face-centred cubic with a lattice constant of 11.34 Å which is close to twice the value of the $D0_3$ lattice constant. This may explain why the Fe–Nb–Si phase crystallizes at the boundaries of Fe–Si grains.

Supposing the new FCC phase to be metallic in character, the high space-filling factor together with the large lattice constant would suggest a unit-cell size containing not less than 100 atoms, if one takes into account the chemical composition of the phase as indicated by Mössbauer spectroscopy and microanalysis. The values of the atomic radii which are necessary for this calculation were taken from Pearson [37]. As a matter of fact, the number of FCC structures having this many atoms in the unit cell is very limited. The four structures which meet the above criterion are listed in table 8.

**Table 8.** Large FCC crystal structures.

| Structure | Prototype | Space group | Atoms |
|---|---|---|---|
| $D2_3$ | $NaZn_{13}$ | $Fm3c$ | 112 |
| $D8_4$ | $Cr_{23}C_6$ | $Fm3m$ | 116 |
| $D8_a$ | $Th_6Mn_{23}$ or $Mg_6Cu_{16}Si_7$ | $Fm3m$ | 116 |
| $E9_3$ | $Fe_3W_3C$ ($\eta$-carbide) | $Fd3m$ | 112 |

The x-ray spectra of these structure types were simulated using a computer program for calculating the diffraction pattern [38] and by filling the respective unit cells with different reasonable combinations of the atoms involved. Only the two structures with space group $Fm3m$ gave a satisfying agreement between experimental and calculated spectra, the simulated $D8_a$ structure fitting the data better than the $D8_4$ structure.

On the grounds of the above results, the new crystalline phase is suggested to have the $D8_a$ structure, the nominal composition being $Fe_{16}Nb_6Si_7$. This structure has five different crystallographic sites by which the results of the microanalysis can be explained if one admits a certain variation in their occupation by the involved atoms.

The $Fe_{16}Nb_6Si_7$ phase is not established in the Fe–Nb–Si ternary phase diagram [39,40], whereas $Co_{16}Nb_6Si_7$ and $Ni_{16}Nb_6Si_7$ are both known to exist [37]. It is possible that the $D8_a$ structure is here stabilized by a certain boron content, which could not be verified due to the lack of sensitivity to light elements of the energy dispersive microanalysis. The stability of this phase may be due to the restricted rate of crystal growth in $Fe_{73.5}Cu_1Nb_3Si_{13.5}B_9$, and its nucleation may depend strongly on the nearly commensurate lattice constant of the $D0_3$ Fe–Si phase.

On the other hand, the report on the Fe–Nb–Si system published by Goldschmidt [39] already includes a phase with unknown stucture marked as $\rho'$ in the section at 1000 °C through the phase diagram near $Fe_{55}Nb_{25}Si_{30}$.

In order to confirm the identity of the new $Fe_{16}Nb_6Si_7$ phase, further studies are necessary including XRD thermal-scan measurements, boron-sensitive microanalysis and electron diffraction. The latter technique could not be performed with the equipment available because, with a conventional (non-scanning) TEM, the minimum area which can be selected for diffraction is as large as $1\mu m$.

### *3.5. Sample E: annealing at 950 °C, 90 h*

After increasing the annealing time at a temperature of $T_a = 950$ °C from 1 h to $t_a = 90$ h, the ribbon revealed the Mössbauer spectrum which is shown in figure 10. The hyperfine parameters of the subspectra are given in table 9.

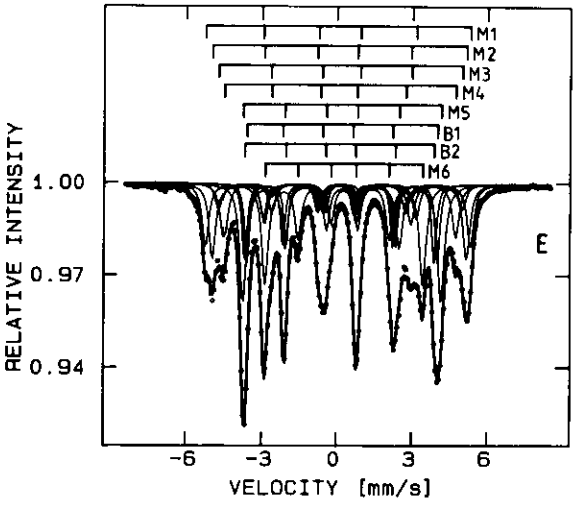


**Figure 10.** Transmission Mössbauer spectrum of sample E: $Fe_{73.5}Cu_1Nb_3Si_{13.5}B_9$ annealed at 950 °C for 90 h.

The thermal treatment discussed in this section was performed mainly to check the stability of the phases which were found in the earlier states of crystallization. Regarding the Mössbauer spectrum, it is evident that the single line S1 has vanished. The $Fe_{16}Nb_6Si_7$ phase is therefore considered to be metastable. $Fe_3Si_{1-x}$ and $Fe_2B$, on the other hand, are equilibrium phases and are still present. Their relative spectral areas have increased, the Fe–Si phase now containing approximately 78 at.% of the iron in the sample and having a silicon content of 19.5 at.%.

**Table 9.** Hyperfine parameters as obtained for sample E: $Fe_{73.5}Cu_1Nb_3Si_{13.5}B_9$, 950 °C/90 h.

| Subspectrum | $\delta$ (mm $s^{-1}$) | QS (mm $s^{-1}$) | H (kOe) | $\Gamma$ (mm $s^{-1}$) | RA (%) |
|---|---|---|---|---|---|
| M1 | 0.07 | −0.03 | 328 | 0.33 | 11.3 |
| M2 | 0.06 | 0.04 | 314 | 0.33 | 13.5 |
| M3 | 0.16 | −0.01 | 302 | 0.33 | 4.5 |
| M4 | 0.09 | 0.02 | 287 | 0.33 | 9.5 |
| M5 | 0.20 | 0.00 | 246 | 0.33 | 21.0 |
| M6 | 0.27 | 0.01 | 196 | 0.33 | 17.7 |
| B1 | 0.12 | 0.09 | 237 | 0.23 | 11.2 |
| B2 | 0.12 | −0.03 | 235 | 0.23 | 11.2 |

The question arises concerning what has happened to the niobium fraction which had been part of the FCC Fe–Nb–Si phase observed in the sample heat treated for only one hour at the same temperature. In figure 11 simultaneous conversion electron Mössbauer spectroscopy (CEMS), conversion x-ray Mössbauer spectroscopy (CXMS) and transmission Mössbauer spectroscopy (TMS) spectra [41] of sample E are plotted.

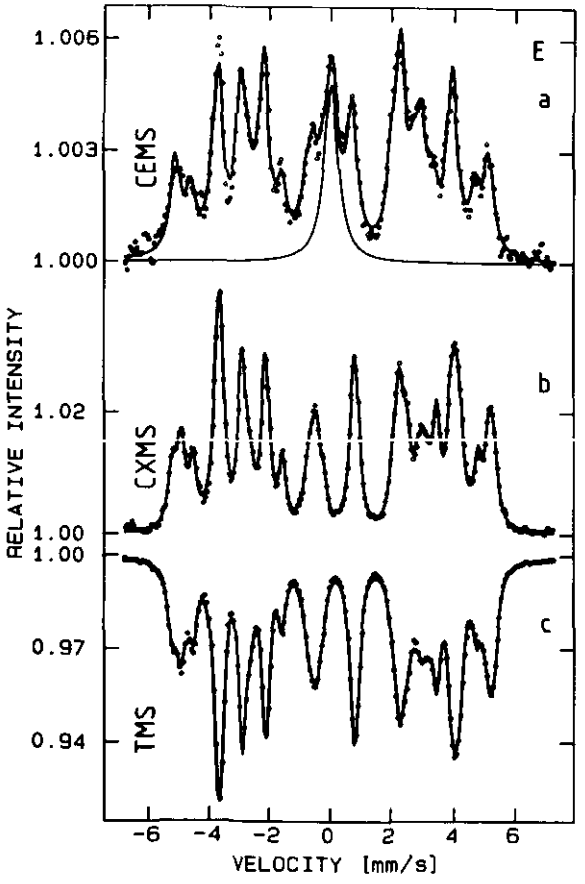


**Figure 11.** Simultaneous CEMS (*a*), CXMS (*b*) and TMS (*c*) spectra of sample E: $Fe_{73.5}Cu_1Nb_3Si_{13.5}B_9$ annealed at 950 °C for 90 h.

For better clarity it should be noted that CEMS and CXMS have a sampling range

of about 0.1 $\mu$m and 10 $\mu$m from the surface, respectively [42], whereas TMS scans the whole sample.

These spectra reveal that the single line which disappeared in the TMS spectrum, is still present in the CEMS spectrum of the surface. This means that there should be a surface layer of a paramagnetic phase. This layer must be very thin, because no single line can be found in the CXMS spectrum.

In order to identify this possible new niobium phase, a SEM/EDX study using instruments by CamScan and Tracor Northern, was undertaken and yielded some rather unexpected results. Figure 12 shows an image which was taken in the backscattered electron mode of the SEM, and figure 13 shows iron, niobium and silicon distribution images.

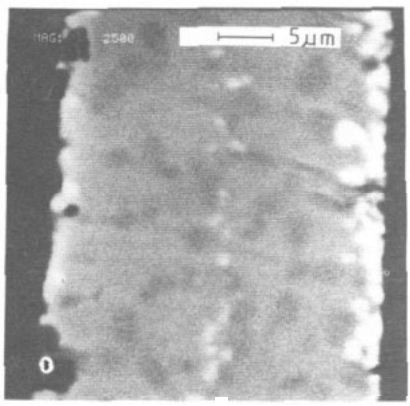


**Figure 12.** SEM image of sample E: $Fe_{73.5}Cu_1Nb_3Si_{13.5}B_9$ annealed at 950°C for 90 h.

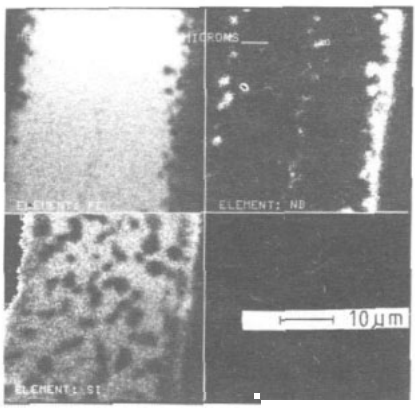


**Figure 13.** Elementary distribution images of sample E: $Fe_{73.5}Cu_1Nb_3Si_{13.5}B_9$ annealed at 950°C for 90 h. Iron, niobium, and silicon distributions are shown.

Obviously, a macroscopic segregation of a phase containing mainly niobium has taken place. A SEM cross section of the sample heat treated only for one hour at the same temperature shows that this segregation is new after the 90 h treatment.

The results of the microanalysis are presented in table 10. No copper was detected, probably because the size of the copper grains is too small for the magnification chosen. The copper grains are believed to remain small during the crystallization process because Cu diffusion is restricted by the low solubility in $DO_3$ Fe–Si.

**Table 10.** Microanalysis of sample E: $Fe_{73.5}Cu_1Nb_3Si_{13.5}B_9$. 950°C/90 h.

| | |
|---|---|
| Fe-Si | **Forming a matrix with a homogenous composition of Fe-15** at.% Si from EDX analysis |
| Fe-B | Some grains of virtually pure Fe detected by EDX were interpreted as boride grains. They appear dark in the backscattering electron mage, because the mean atomic mass is smaller than in the Fe-Si phase |
| Nb-Fe-Si | Microanalysis yields a mean composition of 81 at.% Nb, 17 at.% Fe and 2 at.% Si |

In order to determine the crystal structure of this Nb–Fe–Si phase, an XRD spectrum was recorded using Mo K$\alpha$ radiation. This spectrum is shown in figure 14, and the results are given in table 11.

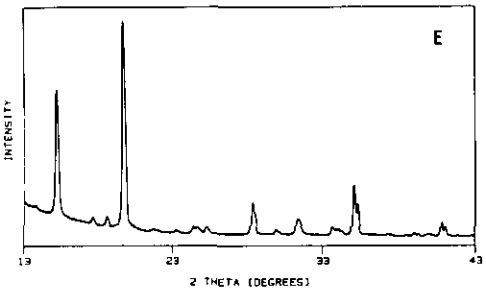


**Figure 14.** XRD spectrum (Mo K$\alpha$ of sample E: $Fe_{73.5}Cu_1Nb_3Si_{13.5}B_9$ annealed at 950°C for 90 h.

**Table 11.** XRD phase analysis for sample E: $Fe_{73.5}Cu_1Nb_3Si_{13.5}B_9$, 950 °C/90 h.

| Phase | Crystal system | Lattice parameters |
|---|---|---|
| $Fe_{3+x}Si_{1-x}$ | Cubic (FCC) | $a = 5.686$ Å ( 17.5 at.% Si) |
| $Fe_2B$ | Tetragonal | $a = 5.140$ Å $c = 4.250$ Å |
| Nb–Fe–Si | Cubic (FCC) | $a = 4.470$ Å |

No copper reflections can be detected, which is again attributed to the smaller grain size of this phase resulting in a loss of intensity relative to the other phases with a larger coherence length.

The $D0_3$ Fe–Si phase has a lattice constant of 5.686 Å, from which the silicon content is calculated to be 17.5 at.% . The peaks belonging to the Nb–Fe–Si phase are very intense due to the fact that this phase is concentrated near the surface of the ribbon, in a region which is comparable in thickness to the penetration depth of the x-ray. This phase turns out to be FCC with a lattice constant of 4.47 Å, where the (111), (200), (220), (311), (222), and (331) reflections are all present. On the other hand, no further peaks could be found indicating any kind of superstructure. The broadening of these peaks is an indication of a certain variation in the lattice constant of this phase.

Taking into account the atomic radius of niobium [37], the unit cell of this structure may contain not more than four niobium atoms. It is therefore proposed to have the most simple FCC structure, the A1 structure. It is possible for atoms as large as an iron atom to occupy intersitial (octahedral) sites in an A1 structure with so large a lattice constant. It is therefore suggested that iron and silicon may be located interstitially.

Again, a phase with the above structure is not known to exist in the ternary system Nb–Fe–Si [39, 40]. It may be stabilized by a certain boron content which cannot be verified using the EDX method. Eggers and Peter [43], however, mention a niobium-rich high-temperature phase with the composition $Nb_{89}Fe_{11}$ and of unknown structure in their report on the binary system Fe–Nb.

Again, further investigations are necessary to confirm the structure of this FCC phase. In the transmission Mössbauer spectrum, the phase cannot be detected because it contains less than 1 at.% of the iron in the sample.

## 4. Conclusion

Annealing of FINEMET $Fe_{73.5}Cu_1Nb_3Si_{13.5}B_9$ at 550 °C for 1 h leads to the favourable nanocrystalline structure of Fe–Si mixed with a remaining amorphous fraction.

Increasing the annealing temperature to 700 °C leads to the formation of $Fe_2B$ and some amorphous remains further depleted in iron, indicated by the resulting single line. There are some indications of the presence of a small amount of $(Fe,Si)_3B$.

A further increase of the annealing temperature to 950 °C leads to a decrease the line width of the single line which is attributed to an FCC Nb–Fe–Si phase. This phase should be the main object of further research. The $(Fe,Si)_3B$ phase has disappeared.

After annealing the ribbon at 950 °C for 90 h, agglomeration of the niobium in a thin surface layer can be observed.

In the Mössbauer phase analysis one must carefully take into account the many subspectra of the ordered $DO_3$ Fe–Si phase. The combination of complementary methods seems to be of great advantage.

The crystallization behaviour of FINEMET $Fe_{73.5}Cu_1Nb_3Si_{13.5}B_9$ remains an interesting subject of further research.

## Acknowledgments

We thank Dr H R Hilzinger, Vakuumschmelze GmbH, Hanau, for providing the amorphous $Fe_{73.5}Cu_1Nb_3Si_{13.5}B_9$ material.

## References

[1] Yoshizawa Y, Oguma S and Yamauchi K 1988 New Fe-based soft magnetic alloys composed of ultrafine grain structure *J. Appl. Phys.* **64** 6044–6

[2] Yoshizawa Y, Yamauchi K, Yamane T and Sugihara H 1988 Common mode choke cores using the new Fe-based alloys composed of ultrafine grain structure *J. Appl. Phys.* **64** 6047–9

[3] Yoshizawa Y and Yamauchi K 1989 Effects of magnetic field annealing on magnetic properties in ultrafine crystalline Fe–Cu–Nb–Si–B alloys *IEEE Trans. Magn.* **MAG-25** 3324–6

[4] Yoshizawa Y and Yamauchi K 1990 Fe-based soft magnetic alloys composed of ultrafine grain structure *Mater. Trans. JIM* **31** 307–14

[5] Köster U, Schünemann U, Blank-Bewersdorff M, Brauer K, Sutton M and Stephenson G B 1991 Nanocrystalline materials by crystallization of metal-metalloid glasses *Mater. Sci. Eng.* A **133** 611–5

[6] Herzer G. 1989 Grain structure and magnetism of nanocrystalline ferromagnets *IEEE Trans. Magn.* **MAG-25** 3327–9

[7] Hilzinger H R 1990 Recent advances in rapidly solidified soft magnetic materials *J. Magn. Magn. Mater.* **83** 370–4

[8] Kataoka N, Inoue A, Masumoto T, Yoshizawa Y and Yamauchi K 1989 Effect of additional Cu element on structure and crystallization behaviour of amorphous Fe–Nb–Si–B alloys *Japan. J. Appl. Phys.* **28** L1820–3

[9] Noh T H, Lee M B, Kim H J and Kang I K 1990 Relationship between crystallization process and magnetic properties of Fe–(Cu–Nb)-Si–B amorphous alloys *J. Appl. Phys.* **67** 5568–70

[10] Kohmoto O, Haneda K and Choh T 1990 Mössbauer effect of Fe–Cu–Nb–Si–B alloys having high permeability *Japan. J. Appl. Phys.* **29** L1460–2

[11] Fujinami M, Hashiguchi Y and Yamamoto T 1990 Crystalline transformations in amorphous $Fe_{73.5}Cu_1Nb_3Si_{13.5}B_9$ alloy *Japan. J. Appl. Phys.* **29** L477–80

[12] Sawa T and Takahashi Y 1990 Magnetic properties of FeCu(3d transition metals)SiB alloys with fine grain structure *J. Appl. Phys.* **67** 5565–7

[13] Jiang J, Aubertin F, Gonser U and Hilzinger H R 1991 Mössbauer spectroscopy and x-ray diffraction studies of the crystallization in the amorphous $Fe_{73.5}Cu_1Nb_3Si_{13.5}B_9$ alloy *Z. Metallk.* **82** 698–702

[14] Krämer A, Jing J and Gonser U 1990 Magnetism of nanocrystalline materials *Hyperfine Interact.* **54** 591–8
[15] Jing J, Krämer A, Birringer R, Gleiter H and Gonser U 1989 Modified atomic structure in a Pd-Fe–Si nanoglass: a Mössbauer study *J. Non-Cryst. Solids* **113** 167–70
[16] Kündig W 1969 A least squares fit program *Nucl. Instrum. Methods* **75** 336–40
[17] Price D C 1981 Empirical Lineshape for Computer Fitting of Spectral Data *Aust. J. Phys.* **34** 51–6
[18] Campbell S J and Aubertin F 1990 Evaluation of distributed hyperfine parameters *Mössbauer spectroscopy applied to inorganic chemistry: Modern Inorganic Chemistry* ed G J Long and F Grandjean vol. 3 (New York: Plenum) ch 4 pp 183–242
[19] Hesse J and Rübartsch A 1979 Model independent evaluation of overlapped Mössbauer spectra *J. Phys. E: Sci. Instrum.* **12** 526–32
[20] LeCaer G and Dubois J M 1979 Evaluation of hyperfine parameter distributions from overlapped Mössbauer spectra of amorphous alloys. *J. Phys. E: Sci. Instrum.* **12** 1083–90
[21] Kubaschewski O 1982 *Iron Binary Phase Diagrams* (Berlin: Springer)
[22] The International Union of X-ray Crystallography. *Structure Report* **9** (1942–1944) 61–2
[23] Yelsukov Y P and Konygin G N 1989 Nuclear gamma resonance spectroscopy of disordered iron–silicon alloys *Phys. Met. Metall.* **67** 87–95
[24] Stearns M B 1963 Internal magnetic fields, isomer shifts and relative abundances of the various fe sites in FeSi alloys *Phys. Rev.* **129** 1136–43
[25] Arita M, Nasu S and Fujita F E 1985 Determination of long-range order parameter of $Fe_3Si$ alloy by means of $^{57}Fe$ Mössbauer effect *Trans. Jap. Inst. Met.* **26** 710–20
[26] Yelsukov Y P, Barinov V A, Galakhov V R and Konygin G N 1985 Kinetics of ordering in alloy $Fe_3Si$ *Phys. Met. Metall.* **60** 83–8
[27] Yelsukov Y P, Barinov V A and Konygin G N 1986 Influence of the order-disorder transition on the structural and magnetic properties of BCC iron–silicon alloys *Phys. Met. Metall.* **62** 85–90
[28] Herzer G 1990 Grain size dependence of coercivity and permeability in nanocrystalline ferromagnets *INTERMAG-90 Conf. (Brighton, 1990)* paper AD-01
[29] Zemčík T, Jirásková Y, Závěta K, Eckert D, Schneider J, Mattern N and Hesske D 1991 Structure, magnetic properties and Mössbauer spectroscopy of amorphous and nanocrystalline $Fe_{73.5}Cu_1Nb_3Si_{16.5}B_6$ *Mater. Lett.* **10** 313–7
[30] Alp E E, Simon K M, Saporoschenko M and Brower W E Jr 1984 Observation of crystallisation in $Fe_{80}B_{20}$ metallic glass by DSC and Mössbauer spectroscopy *J. Non-Cryst. Solids* **61** 871–6
[31] Limbach C T, Aubertin F and Gonser U 1988 Observation of crystallization in $Fe_{80}B_{20}$ metallic glass by DSC and Mössbauer spectroscopy *Physica* B **149** 263–6
[32] Fasiska E J and Jeffrey G A 1965 On the cementite structure *Acta Cryst.* **19** 463–71
[33] Ron M and Mathalone Z 1971 Hyperfine interactions of $^{57}Fe$ in $Fe_3C$ *Phys. Rev.* B **4** 774–7
[34] Schaaf P, Wiesen S and Gonser U 1992 Mössbauer study of iron-carbides: Cementite $(Fe,M)_3C$ with various manganese and chromium contents *Acta Metall.* **40** 373–9
[35] Choo W K and Kaplow R 1977 The distinctness of magnetic hyperfine fields associated with structurally unique iron sites in $Fe_3B$ *Metall. Trans.* A **8** 417–9
[36] Aronsson B and Lundgren G 1959 X-ray investigations of the Co–Si–B system at 1000 °C. Intermediate phases in the Co–Si–B and Fe–Si–B systems *Acta Chem. Scand.* **13** 433–41
[37] Pearson W B 1972 *The Crystal Chemistry and Physics of Metals and Alloys* (New York: Wiley)
[38] Yvon K, Jeitschko W and Parthé E 1969 *A Fortran IV program for the intensity calculation of powder patterns* University of Pennsylvania, Laboratory for Research on the structure of matter, Pennsylvania
[39] Goldschmidt H 1960 The constitution of the iron–niobium–silicon system *J. Iron Steel Inst.* **194** 169–80
[40] Raghavan V and Gosh G 1984 The Fe–Nb–Si (iron–niobium–silicon) system *Trans. Indian Inst. Met.* **37** 421–5B
[41] Gonser U, Schaaf P and Aubertin F 1991 Simultaneous triple radiation Mössbauer spectroscopy (STRMS) *Hyperfine Interactions* **66** 95–100
[42] Wagner F E 1976 Applications of Mössbauer scattering techniques *J. Physique* **37** C6 673–89
[43] Eggers H and Peter W 1938 Das Zustandsdiagramm Eisen–Niob *Mitt. Kaiser-Wilh.-Inst. Eisenforsch.* **20** 199–203